Modeling of Structural Properties of Zr(Nb)-Doped c-LTO–Zr(Nb) Materials With Spinel Structure for Li-Ion Batteries

MIRSALIM M. ASADOV[1, 2,*], SOLMAZ N. MUSTAFAEVA[3], SAIDA O. MAMMADOVA[3],
ESMIRA S. KULI-ZADE[1], VLADIMR F. LUKICHEV[4]
[1]Nagiyev Institute of Catalysis and Inorganic Chemistry,
Ministry of Science and Education of Azerbaijan,
Baku, AZ-1143,
AZERBAIJAN

[2]Scientific Research Institute of Geotechnological Problems of Oil, Gas and Chemistry,
Ministry of Science and Education of Azerbaijan,
Baku, AZ-1010,
AZERBAIJAN

[3]Institute of Physics, Ministry of Science and Education of Azerbaijan,
Baku, AZ-1143,
AZERBAIJAN

[4]Valiev Physics and Technology Institute,
Russian Academy of Sciences,
Moscow, 117218,
RUSSIA

**Corresponding Author*

Abstract: - Using the density functional theory (DFT), we investigated the electronic, magnetic and energy properties of $Li_4Ti_{5-x}M_xO_{12}$ (M = Zr, Nb; x = 0–0.01) (or c-LTO–Zr (Nb)) supercells, which are isostructural to the high-temperature spinel (cubic; sp.gr. $Fd\bar{3}m$) modification of the $Li_4Ti_5O_{12}$-based anode material (c-LTO) for lithium-ion batteries (LIB). In DFT calculations with a generalized gradient approximation (functional GGA), spin-orbit coupling (SOC) and the Hubbard correction were considered (DFT SGGA+ U). For the Ti 3d and Zr(Nb) 4d states, pd and dd-model values of the U effective interaction energies were used. To account for the effective Coulomb intra-atomic interaction (U) between particles, the DFT SGGA+U calculations were performed using U_{eff} = 4 eV, O 2p, Ti 3d, Zr (Nb) 4d. The band structure and density of states (DOS) of c-LTO supercells calculated by DFT SGGA+U are consistent with both theoretical and experimental data for c-LTO. The theoretical band gap (E_g) is smaller than the experimental value of c-LTO. Taking into account the chemical potentials of the doping impurities, the formation energy of c-LTO–Zr(Nb) was calculated. The decrease in the total energy due to the change in the partial densities of states (PDOS) of the filled spin-up and spin-down subbands indicates that c-LTO–Zr(Nb) is thermodynamically stable. The density of spin-up d-states exceeds the density of spin-down d-states in c-LTO–Zr(Nb), so the E_g values in these structures differ from each other. Doping with Zr(Nb) narrows E_g and improves the electrical conductivity of c-LTO–Zr(Nb) due to the contribution of Zr^{4+} 4d and Nb^{3+} 4d orbitals to the particle transport. The Fermi level of the band structure of c-LTO–Zr(Nb) supercells shifts to the conduction band as a result of Zr(Nb) doping. The local magnetic moments of Zr(Nb) impurity atoms in c-LTO–Zr(Nb) are calculated.

Key-Words: - New Battery Materials, Doped Lithium Titanate Oxide, c-LTO–Zr(Nb), Density Functional Theory, DOS, Band Structure, Magnetic Moment.

Received: April 30, 2024. Revised: November 11, 2024. Accepted: December 1, 2024. Published: December 31, 2024.

1 Introduction

Rechargeable lithium-ion batteries (LIBs) are known to be alternative energy storage systems. LIBs provide high energy density and long cycle life, making them important for applications such as portable electrical appliances, [1], [2], [3], [4], [5]. The power of LIBs depends on various electrode materials and factors, including the rate of lithium-ion and electron migration through the electrolyte between the two electrodes. To produce high-power and stable LIBs, it is necessary to develop new materials and highly conductive nanostructures for the electrodes. Graphite, graphene, and lithium titanate oxide $Li_4Ti_5O_{12}$ (c-LTO), in particular with a nanocrystalline spinel structure (face-centered cubic syngony; space group $Fd\bar{3}m$; $a \approx 8.35$ Å), are used as anode materials. Such electrode nanomaterials accelerate the transport of particles in LIBs and ensure their stability.

In order to increase the service life of LIB, new materials are being developed that effectively reduce energy losses caused by battery polarization. Materials such as c-LTO increase the service life of LIB, compared to graphite materials, [6].

LTO can operate at high current densities corresponding to the 60C mode, when charging and discharging occur in 1 min. In this case, the decrease in LIB capacity is ~ 50% of the nominal capacity. LTO has good cyclability due to the same specific volume in the LIB charge/discharge process. The oxidized and reduced compositions of c-LTO and $Li_7Ti_5O_{12}$ at the phase boundary of the c-LTO spinel phase have an almost horizontal discharge curve. This is due to the two-phase discharge mechanism and low mutual solubility of c-LTO/$Li_7Ti_5O_{12}$ at the boundary of the spinel phase (111). One of the disadvantages of c-LTO as a negative electrode (anode during discharge) in LIB is its relatively low theoretical specific capacity of 175 mAh/g (for graphite this value is 372 mAh/g).

The reversible process of lithium implantation in c-LTO at the phase boundary of the c-LTO/$Li_7Ti_5O_{12}$ spinel phase (111) reduces the oxidation state of titanium from Ti^{+4} to $Ti^{+3.4}$ in batteries. This process in LIB takes place at a potential of +1.5 V according to the reaction:

$Li_4Ti_5O_{12}$ (spinel) + 3 Li^+ + 3e ↔ $Li_7Ti_5O_{12}$ (rock salt). (1)

The parameters of the crystal lattice of c-LTO, as a negative electrode, do not change significantly in this process. Titanium ions can also be reduced to the oxidation state of Ti^{+3} by increasing the concentration of implanted other ions, including lithium ions in the c-LTO electrode. The theoretical specific capacity of LIB in this process with lithium-ion increases to 290 mAh/g. However, such reactions with other metal ions can cause irreversible structural changes in the c-LTO electrode, and its capacity can decrease during LIB cycling. Therefore, improving the characteristics of the electrodes (increasing the electron conductivity of the achieved discharge capacity, and reducing material degradation during LIB cycling) is a practically important task. For example, by doping c-LTO, it is possible to introduce d-element ions into the c-LTO lattice and reduce titanium ions to Ti^{+3} without destroying the c-LTO lattice.

Doping of c-LTO with lanthanides (Eu [3], La [4], [5], [6], [7], [8], [9], [10], [11], [12], [13], Pr [14], Nd [15]) can increase the discharge capacity and cycling stability over a wide potential range. However, the effect of doping with transition *d*-elements on the electrochemical properties of c-LTO has been little studied.

The results of the study of Zr doping of c-LTO compound with a cubic structure at the Ti site show that the electrochemical performance of the $Li_4Ti_{5-x}Zr_xO_{12}$ electrode is improved, [16], [17], [18]. The reduction of titanium ions $Ti^{+4} \rightarrow Ti^{+3}$ in the c-LTO electrode can also be achieved by Nb doping at the Ti site of the c-LTO lattice [19], [20]. This can increase the charge transfer efficiency of $Li_4Ti_{5-x}Nb_xO_{12}$, which in turn will improve the performance of LIB.

Our work [17] presents the results of ab initio modeling of the monoclinic modification of m-LTOZr(Nb) (sp. gr. $C2/c$, No. 15; a = 8.35 Å, b = 8.32 Å, c = 13.17 Å). Zr(Nb) doping of the m-LTO crystal in the lithium position enhances the spin-orbit interaction in the electronic structure of m-LTO–Zr(Nb). And this, in turn, can increase charge transfer and improve LIB performance. However, there is still no data on the electronic structure of c-LTO–Zr(Nb) crystals with a cubic structure.

The aim of this work is ab initio modeling of the structural properties of Zr(Nb)-doped (x = 0-0.01 mole fraction) c-LTO–Zr(Nb) materials with a cubic structure (space group $Fd\bar{3}m$) for LIB. Changes in the electronic band structure and energy of doped c-LTO–Zr(Nb) nanocrystals with changes in composition and structure were studied using ab initio methods with the Hubbard correction. Supercells were considered in which the interaction of impurity Zr(Nb) atoms partially substituting for

titanium atoms leads to changes in the properties of c-LTO–Zr(Nb).

2 Calculation Methods

Below are the results of studying the change in the electronic structure and energy of doped c-LTO–Zr(Nb) nanocrystals under light doping conditions. The electronic band structures of c-LTO–Zr(Nb) of the cubic modification were calculated using density functional theory methods taking into account spin polarization and the Hubbard correction (DFT SGGA+U). The c-LTO–Zr(Nb) supercells are considered, in which titanium particles are partially substituted by Zr(Nb) particles in the cell. For $Li_4Ti_{5-x}Zr_xO_{12}$ and $Li_4Ti_{5-x}Nb_xO_{12}$, the impurity concentration was in the range x = 0–0.01. The structural parameters of the crystals were calculated without taking into account van der Waals interactions and the U correction. The interaction of impurity Zr(Nb) particles with partial substitution of titanium in the c-LTO cell does not qualitatively change the lattice parameter of c-LTO–Zr(Nb) crystals. The use of ab initio methods allows us to compare and predict the physical and physicochemical properties of c-LTO–Zr(Nb) materials. Using the example of DFT GGA–PBE [21], [22], [23] calculation of the electronic properties of binary and ternary phases in [24], we present a method for calculating the characteristics of anode materials. In [25], the electronic-structural and physical properties of partially doped SiC–Li supercells were calculated for LIB.

The DFT method with the local density approximation (LDA) functional is not able to adequately predict the parameters of materials. The DFT LDA calculation leads to an incorrect metallic state, for example, for transition metal oxides. In LDA, the exchange-correlation functional (XC) depends only on the density (ρ) in the coordinate $(\mathbf{r})$ where it is calculated:

$$E_{\mathrm{XC}}^{\mathrm{LDA}}(\rho) = \int E_{\mathrm{XC}}(\rho)\rho(\mathrm{r})d^3\mathbf{r} \qquad (2)$$

The c-LTO object is an example of a ternary compound in which titanium ions contain partially filled *d*-orbitals. In doped c-LTO, the DFT LDA calculations show a metallic state of the electronic structure of c-LTO. On the other hand, the LDA functional in the calculations underestimates the lattice constants of the crystal and overestimates the binding energies. In other words, the preliminary DFT LDA calculation reduced the accuracy of the calculation. In addition, LDA functional is ineffective in calculations for predicting equilibrium configurations of surface and defect structures, in particular, oxide materials.

Taking this into account, a modified LSDA functional was used in the calculations, including the spin-orbit interaction (SOC) for the atomic electron:

$$E_{\mathrm{XC}}^{\mathrm{LSDA}}(\rho_\uparrow, \rho_\downarrow) = \int E_{\mathrm{XC}}(\rho_\uparrow, \rho_\downarrow)\rho(\mathrm{r})d^3\mathbf{r} \qquad (3)$$

In DFT calculations of the energy of c-LTO-based structures, in addition to those indicated, the effect of the Hubbard Coulomb repulsion energy (U) on the total energy was also taken into account. Total energy calculations were performed using GGA–PBE software, [17], [24]. The use of the LSDA+U functional improved the results of calculations of the electronic structure of c-LTO–Zr and c-LTO–Nb materials. These structures are characterized by strong electronic interactions in spatially localized states, in particular, *d*-orbitals, of Zr(Nb) alloying components. Adding the correction term U to the single-particle electronic potential increases the accuracy of calculations.

DFT LSDA+U calculations of c-LTO–Zr(Nb) supercells yield a smaller band gap E_{g} than the experimental value. Increasing the size of c-LTO–Zr(Nb) supercells does not improve the calculated E_{g} value compared to the experimental value c-LTO. DFT LSDA+U calculated E_{g} were still smaller than the experimental E_{g} value.

Taking into account the above, the generalized gradient approximation (GGA) functional was used in the calculations. The GGA potential adds a term to the DFT calculations that reflects the electron density gradient at a given point. In DFT GGA calculations, the non-uniform distribution of electron density and non-local effects are partially taken into account. DFT SGGA+U calculations of c-LTO–Zr(Nb) parameters were closer to experimental data compared to DFT LSDA+U calculations.

In the DFT SGGA+U calculations, the basic electron configurations of the components in the following valence states were used: Li – $1s^22s^1$, O – $1s^22s^22p^4$, Ti – [Ar] $3d^24s^2$, Zr – [Kr]$4d^25s^2$, Nb – [Kr] $4d^45s^1$. The effect of *d*-orbitals of Zr(Nb) doping of c-LTO was taken into account in the calculations by the SOC contribution to the electronic structure. In other words, partial substitution of titanium in the c-LTO lattice by doping Zr(Nb) metal atoms was taken into account in the calculations by the SOC term.

For the analysis of c-LTO–Zr(Nb) systems and for the calculation of the total potential, we used the effective Hubbard parameter as $U_{\text{eff}} = U - J$, where the constant $J = 0$. In other words, for the analysis of Ti 3d and Zr(Nb) 4d states taking into account the occupation number of d-orbitals in the calculation parameter U_{eff}, the constant was taken as $J = 0$.

In the DFT SGGA+U calculations, the contribution of the local Coulomb repulsion between localized d-electrons was taken into account by the effective Hubbard energy U_{eff} = 4 eV. The kinetic energy of plane wave cutoff was 300 eV. In the supercell calculations, a k-grid scheme constructed using the Monkhorst–Pack method was used, and a flat grid with dimensions of 2 × 2 × 2 in the Brillouin zone was chosen. Increasing the k-grid size in the irreducible wedge of the first Brillouin zone of supercells using nonequivalent k-points does not have a significant effect on the experimental lattice parameters and atomic positions in the calculations. The unit cell parameters and atomic positions in the c-LTO–Zr(Nb) lattice were optimized. The atomic positions and cell parameters were determined by relaxing all forces in the system to ≤ 0.01 eV/Å. Each alloying element was considered as a substitutional defect in the 32-atom c-LTO–Zr(Nb) supercell. The formation energy was determined by the formula:

$$E_f(\text{X}) = E(\text{X}) - E(\text{bulk}) - \mu_{\text{X}} + (\tfrac{1}{4})\mu_{\text{Li}} + (\tfrac{1}{5})\mu_{\text{Ti}} + (\tfrac{1}{12})\mu_{\text{O}}, \quad (4)$$

where (X) and $E(\text{bulk})$ are the total energy of the supercell with c-LTO–Zr(Nb) and without the alloying element Zr(Nb), μ_{X}, μ_{Li}, μ_{Ti} μ_{O} are the chemical potentials of the alloying element Zr or Nb, Li, Ti and oxygen O, respectively. These values were extracted from the total energy of each element in its stable phase. For these calculations, the Brillouin zones are selected using a k-point grid with a density of at least 5000 points per inverse atom.

3 Results and Discussion

3.1 Li–Ti–O System

When working with phase diagrams of ternary systems, the following interrelated problems are solved: a) the chemical composition of the ternary alloy ABC (or chemical compound ABC) is determined by the position of the figurative point on the plane of the concentration triangle of the system A–B–C; b) the figurative point on the plane of the concentration triangle A–B–C is determined by the specified composition of the ternary alloy ABC. In our case, to analyze the equilibrium state of ternary compounds (or phases) in Li–Ti–O alloys, it is important to consider the quasi-binary section Li_2O–TiO_2. The composition-property section diagram of Li_2O–TiO_2 includes several ternary phases of stoichiometric composition.

The phase diagram of the system contains four ternary compounds, [17]. Figure 1 (Appendix) shows our refined equilibrium phase diagram of the Li–Ti–O system.

The LTO compound is one of the four ternary intermediate phases in the Li–Ti–O system. The LTO compound has several modifications (in particular, monoclinic (m) and cubic (c) structure). No noticeable deviation from the stoichiometry of the LTO composition is observed. The temperature of the phase transition from the monoclinic structure to the high-temperature cubic structure m-LTO → c-LTO is ~930 °C. As indicated above, we are interested in the properties of c-LTO with a spinel structure (cubic structure; space group $Fd\bar{3}m$).

3.2 Formation Energies

The formation energy of chemical bonds determines the stability of the phase. Therefore, the formation energy of the alloyed c-LTO–Zr(Nb) phases was calculated. The outer level of Zr $4d^2 5s^2$, Nb $4d^4 5s^1$ contains four and three electrons, respectively, located on the 4d and 5s sublevels. For Zr and Nb, the oxidation state of +4 and +3, respectively, is more typical, since a small amount of energy must be spent to excite these atoms, i.e. to transfer electrons from the 4d state to the 5s state. This is completely covered by the formation energy of chemical bonds of the alloyed c-LTO–Zr(Nb) phases. The ionization potential of Zr and Nb (free atom) is 6.84 and 6.88 eV (small), the values of electron affinity (0.43 and 0.89 eV) and electronegativity (1.33 and 1.6 on the Pauling scale) are also small. Therefore, Zr and Nb, being active metals, will exhibit reducing properties in the alloying reaction of c-LTO. That is, Zr and Nb atoms will give up electrons when interacting with c-LTO.

Thus, it can be expected that doping will lead to the formation of c-LTO–Zr(Nb) stable molecule. That is, energy is required to break such a molecule. The formation of a chemical bond reduces the

energy of the system, since the bonding pair of electrons is attracted simultaneously by both the nucleus of the cation atoms (Li, Ti, Zr, Nb) and the nucleus of the oxygen atom (O) in c-LTO–Zr(Nb). In this case, the electrons will be distributed unevenly. Since different cation and oxygen atoms will attract electrons with different strengths. This is also determined by the ionization energies of these four different component atoms of c-LTO–Zr and c-LTO–Nb.

In cases where the thermal and volume effects of the reaction are large, i.e. when the energies of formation of chemical bonds have values of the order of 10 kJ/mol, the concentration of doping atoms must be taken into account in the calculations.

In general, the formation energy E_f (or enthalpy of formation $\Delta_f H$) of the c-LTO–Zr(Nb) compound, taking into account equation (1) and individual components (i), is determined by the formula:

$$E_{\text{form}} = E_{\text{total}} - \sum_i E_{\text{total}}(i) \quad (5)$$

$$E_f(\text{c}-\text{LTO}-\text{Zr(Nb)}) \approx \Delta_f H = E(\text{c}-\text{LTO}-\text{Zr(Nb)})_{\text{total}}^{\text{GGA}+U} - E(\text{c}-\text{LTO})_{\text{total}}^{\text{GGA}+U} - \sum_i \mu_i x_i, \quad (5a)$$

where μ_i is the chemical potential of element-component i, x_i is the amount of element i in the c-LTO–Zr(Nb) compound. The methodical part above indicated that as a standard it is accepted that the chemical potential of each species is in the ground state of the element in the DFT calculation of the total energy. The formation energy calculated with this choice is valid for a temperature of 0 K.

The DFT+U calculation included Coulomb interactions in localized d-orbitals with a U correction. Then, taking into account the GGA+U functional, the total energy can be determined from the known expression:

$$E_{\text{total}}^{\text{GGA}+U} = E_{\text{total}}^{\text{GGA}} + \frac{\bar{U}-\bar{J}}{2} \sum_\sigma [(\sum_m n_{m,m}^\sigma) - (\sum_{m,m'} n_{m,m'}^\sigma, n_{m'm}^\sigma)], \quad (6)$$

where $\bar{U}$ and $\bar{J}$ are the spherically averaged matrix elements of the on-site Coulomb interactions of the 3d-orbital, n is the filling matrix of the 3d-orbital at the on-site, obtained by projecting the wave function onto the 3d atomic states. Here m or $m' = -2$, -1,0,1,2 are different d-orbitals, σ =1 or -1 is the electron spin. The site occupancy matrix was expressed in explicit spin and orbital representation. The calculated total energies were insensitive to $\bar{J}$.

To take into account the Hubbard correction U to the GGA functional in DFT calculations in the Coulomb repulsion effect, we neglected the secondary effects of the Coulomb and magnetic interactions. In other words, the parameter J describing these effects was taken equal to zero, $U_{\text{eff}} = U - J$. In this case, the $U \approx U_{\text{eff}}$ correction to the energy functional, significantly simplifies the DFT SGGA+U calculation equations.

The value of $\Delta_f H$ of ternary compounds of the quasi-binary system $TiO_2 - Li_2O$ was calculated by DFT LSDA method, [17]. To calculate the total energy of the compounds, the reference values of $\Delta_f H_{298}^0$ of the corresponding binary oxides of the Li–Ti–O system were used. For binary oxides of titanium and lithium, the following values of $\Delta_f H_{298}^0$ (kJ/mol) were adopted: -1518 (Ti_2O_3), -943 (TiO_2), - 68 (LiO), -598 (Li_2O). DFT GGA + U calculations of the E_f showed a value that is ~0.1 eV higher than the value obtained from DFT LSDA calculations E_f = -3.21 eV, [17].

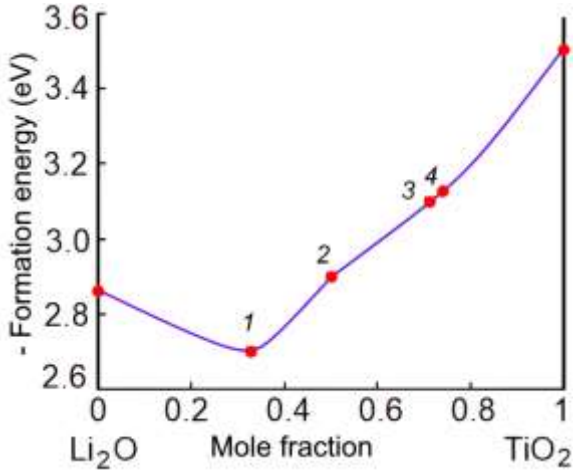

Fig. 2: Formation energy of ternary oxides as a function of the composition of the $Li_2O - TiO_2$ system in DFT SGGA+U (U_{eff} = 4 eV) calculations. *1* – Li_4TiO_4, *2* – Li_2TiO_3, *3* – $Li_4Ti_5O_{12}$, *4* – $Li_2Ti_3O_7$

The DFT SGGA+U (U_{eff} = 4 eV, O 2p-, Ti 3d-, Zr 4d- and Nb 4d-orbitals) formation energy of the ternary compounds Li_4TiO_4 (*1*), Li_2TiO_3 (*2*), $Li_4Ti_5O_{12}$ (*3*) and $Li_2Ti_3O_7$ (*4*) is shown in Figure 2.

These negative E_f values indicate that the ternary compounds are stable in the solid state. Calculated DFT SGGA+U (U_{eff} = 4 eV) formation

energy for $Li_4Ti_{4.99}Zr_{0.01}O_{12}$ and $Li_4Ti_{4.99}Nb_{0.01}O_{12}$ is –3.11 eV.

The difference in E_f can be related to the used LSDA [17] or SGGA+U functional and the change in the distribution of Ti particles and Zr(Nb) alloying particles in the octahedral and tetrahedral voids of the c-LTO–Zr(Nb) cell.

3.3 Atomic Structure of c-LTO

In the spinel structure of c-LTO, oxygen ions (32e) form a cubic close-packed (ccp) array [4]. And the gaps in the crystal lattice are partially occupied by Li and Ti cations with tetrahedral (8a, 8b, 48c) and octahedral (16c, 16d) coordination (Table 1). The atomic structure of the c-LTO cell is shown in Appendix in Figure 3(a) and Figure 3(b).

Table 1. Structural parameters of c-LTO

Atom	Position	Atom coordinates		Occupancy
Li1	8a	0		1.000
Li2	16d	0.625	0.503	
Ti	16d	0.625	0.497	
O	32e	0.389	1.000	

The calculated structural parameters of the relaxed lattice of c-LTO are consistent with the known data. For example, the DFT SGGA calculated lattice parameter a = 8.3523 Å is in good agreement with the data 8.3525 Å, [26].

3.4 Electronic Structure of c-LTO

The theoretical atomic parameters of a chemical compound and the contributions to the chemical bond and electron structure calculated on their basis depend on the choice of the theoretical difference of the exchange integrals for *s*-, *p*- and *d*-electrons. In the considered c-LTO compound, this can be *s*-*p*-*d*-local exchange interactions (*s*-*p*-*d*-model).

In the band structure calculations of the c-LTO system, a difference in energy was found between the spin "up ↑" and spin "down ↓" states. Recall that each atom consists of protons and neutrons, as well as orbiting electrons in a chemical compound. Therefore, if we assume that these atoms have a spin quantum number of ½, then the protons can also exist in two spin states: spin "up" and spin "down". The protons of the atoms have a positive charge and can generate magnetic dipole moments. When a magnetic field is applied to the dipole of a proton, the dipole will either align itself "parallel" or "antiparallel" to the direction of the magnetic field depending on its spin state.

The "parallel" (low energy) and "antiparallel" (high energy) states have a difference in energy (ΔE) which is known to be proportional to the magnetic field strength (B_0), the gyromagnetic ratio (γ) and Planck's constant (h):

$$\Delta E = \gamma \cdot B_0 \cdot (\frac{h}{2\pi}). \quad (7)$$

The ratio of the number of nuclei in states with high (N_{high}) and low (N_{low}) energy is determined as a function of the difference in energy levels (ΔE), the temperature (T) of the system and the Boltzmann constant (k_B):

$$N_{\text{high}}/N_{\text{low}} = \exp[-\frac{\Delta E}{k_B \cdot T}]. \quad (8)$$

The results of DFT SGGA calculations of the electronic structure of c-LTO are analyzed by comparing the band structure and density of states (DOS and partial PDOS) of c-LTO with the known calculated data (E_g = 2 eV [26]). The band gap of c-LTO, found experimentally by extrapolating the linear part of the UV-visible spectra to the energy axis, is 3.55 eV, [27].

The results of DFT SGGA calculations of the electronic structure of c-LTO are analyzed by comparing the band structure and density of states (DOS and partial PDOS) of c-LTO with the known calculated data (E_g = 2 eV [26]). The band gap of c-LTO, found experimentally by extrapolating the linear part of the UV-visible spectra to the energy axis, is 3.55 eV, [27].

As can be seen, the theoretical band gap obtained by us with the single-electron approach using DFT GGA was significantly smaller than the experimental value. To overestimate the calculated band gap of c-LTO, large computational resources are required. More precisely, for such systems (insulators and semiconductors), a significant increase in the unit cell is necessary, so they require a corresponding increase in computational resources. The theoretical band structure of c-LTO calculated with two potentials is shown in Figure 4 (Appendix).

Taking into account the U correction in the calculations of the c-LTO band structure does not significantly increase the value of E_g. In the band structure, the forbidden band is located between the occupied *p*-states of oxygen and the half-empty *d*-states of Ti.

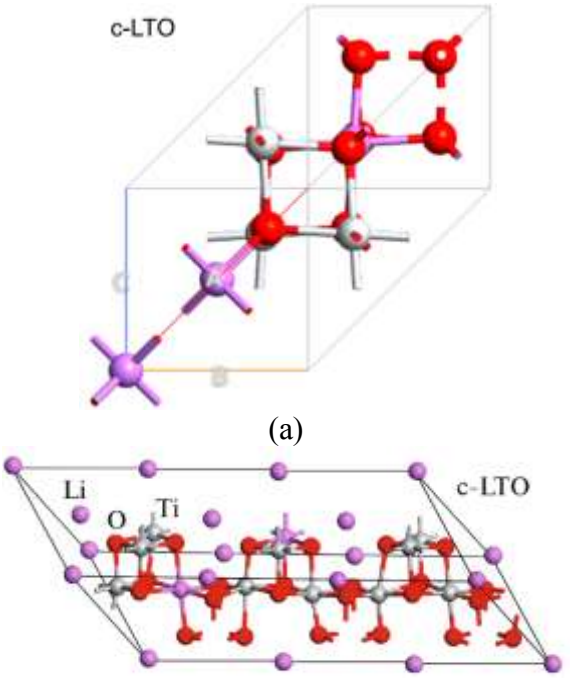

Fig. 3: Atomic structure of c-LTO: primitive unit cell (a), crystal structure (b)

DFT SGGA calculations of E_g values were performed for both spin-up $E_g\uparrow$= 2.34 eV and spin-down $E_g\downarrow$=2.19 eV electron states.

The energy gap is mainly determined by the occupied O 2*p* states and Ti 3*d* states in the c-LTO lattice. DFT SGGA+*U* (U_{eff} = 4 eV, O 2*p*, Ti 3*d*) calculations yield $E_g\uparrow$= 3.56 eV, $E_g\downarrow$ = 2.4 eV for c-LTO.

The theoretical densities of electron states of the c-LTO supercell calculated with the SGGA+*U* potential are shown in Figure 5 (Appendix). From the DOS analysis it follows that the valence band of c-LTO consists mainly of *p*-orbitals of O and *d*-orbitals of Ti with a small admixture of ~~s~~s-orbitals of the components. In the conduction band of the DOS, the *s*- and *p*-orbitals approximately coincide.

In Figure 5 (Appendix), along with the spin-resolved with full DOS, the partial densities of the state of Ti atoms of the c-LTO compound. The PDOS shows sharp peaks at 2 and 4.2 eV, which arise from the ground spin states of Ti. These Ti $3d^2$ states are highly localized since their energy width is small. The minority spin *s*-, and *p*-states of Ti are insignificant and are limited to the energy range from −16 to 16 eV.

The energy characteristics indicate that in c-LTO, the highest occupied molecular orbital is mainly composed of oxygen (*p*-orbital). And the lowest unoccupied molecular orbital is composed of titanium (*d*-orbital). This makes the electronic structure of c-LTO similar to insulators.

Thus, the valence band of c-LTO mainly consists of O 2*p* states, while the conduction band is dominated by the Ti 3*d* orbital states. The overlap of Ti 3*d* and O 2*p* orbital states in DOS indicates a strong O-Ti interaction in the TiO_6 octahedra of the c-LTO lattice.

3.5 Electronic Structure of c-LTO–Zr

There are several grades of cubic c-LTO powders, differing in their properties. The differences in properties are due to the structure of c-LTO grains grown under different thermodynamic and kinetic conditions. The formation of properties is associated with the crystal structure and electronic interaction of the particles of the substance.

Control over the type, and concentration of point defects and impurities, as well as the dislocation structure, enables the creation of crystalline materials with specified properties. However, the known technologies for the synthesis of c-LTO do not fully allow the influence of impurities on the properties to be controlled during crystal growth. There are few works in the literature devoted to the study of the electronic structural properties of doped c-LTO. The parameters of the crystal structure and electrochemical properties of materials based on c-LTO are analyzed.

It can be assumed that the 4*d*-element impurities Zr(Nb) do not have a significant effect on the stoichiometry of c-LTO and the parameters of the crystal structure when substituting the 3*d*-element titanium. The sizes of Zr (atomic radius 1.60 Å; ionic.

Radius 0.79 Å) and Nb (atomic radius 1.46 Å; ionic radius 0.69 Å) are close to the sizes of the substituted titanium (atomic radius 1.47 Å; ionic radius 0.94 Å). In other words, Zr(Nb) impurities should form substitution solutions in c-LTO. An increase in the impurity concentration can distort the cubic lattice of c-LTO and reduce its symmetry. A characteristic difference between the substituted c-LTO–Zr(Nb) material and pure c-LTO is the small contribution of Zr(Nb) 4*d*-orbitals to the zone structure.

In doped c-LTO–Zr(Nb) materials, in addition to the electron charge, we used its spin to control currents. The addition of 4d elements to c-LTO supercells was carried out using the known technique, [17]. The parameters of the crystal structures of the alloying Zr(Nb) atoms and their

atomic (ionic) radii differ from the parameters of c-LTO. Therefore, the solubility of Zr(Nb) atoms in c-LTO was taken to be several percent. That is, it was assumed that c-LTO–Zr(Nb) forms dilute solid solutions, where Zr(Nb) substitutes Ti. Determining the substitution coefficient of Ti for Zr(Nb) in c-LTO is a separate problem. Its solution will allow us to establish where Zr(Nb) is located in the c-LTO lattice sites when Ti is substituted.

The composition, properties, and electronic structure of c-LTO are known, but there is still no consensus on the type of exchange interaction of particles upon doping c-LTO. Approaches to calculating the electronic properties of doped c-LTO include various modifications of the electron density functional method.

The band structure models of c-LTO–Zr(Nb) can be related to the relative energy positions of the Fermi level (E_F), the valence band, and the impurity band, i.e. the band formed by the 4*d* electrons of the Zr(Nb) impurity. In the double exchange model, the *d* level of the transition metal Zr(Nb) should be in the band gap, and in the *p-d* exchange model, the *d* level should lie below the edge of the valence *p* band. In such materials, the Fermi level can be in the impurity band, and by changing its position, the properties of the material can be altered. However, the 4*d* electrons of Zr(Nb) can also hybridize with the valence band at low binding energies (less than 4 eV).

Thus, taking into account also the known experimental data (resonance photoemission, photoelectron spectroscopy, infrared optical data, etc.), we can conclude the following. The 4*d* states of Zr(Nb) impurities can be located both in the valence band of the initial c-LTO and correspond to the *s-d, p-d, and s-p-d* of local exchange interaction models. In this case, the maximum valence band of c-LTO can be near E_F and hybridized with the impurity 4*d* states of Zr(Nb). That is, the Fermi level can be in the impurity band of Zr(Nb), and it is possible that it overlaps with the valence band. In semiconductors, for example, the impurity band and the band of the initial semiconductor are mixed and overlap. Therefore, the valence band and impurity band of the c-LTO–Zr(Nb) structures can be taken as conditional for analysis.

Based on the electronic structure of c-LTO, it can be assumed that after doping, the *d*-states of Ti should be partially filled. Such filling of the *d*-state of Ti can also take place, for example, after Li-intercalation of c-LTO. Then, taking into account the model of the two-phase coexistence of the c-LTO/$Li_7Ti_5O_{12}$ phases (Figure 6, Appendix), it can be assumed that near the spinel phase (111) the structure will have a metallic character.

The energy of this phase boundary of c-LTO/$Li_7Ti_5O_{12}$ calculated by the DFT GGA+U method is small since even nanosized Li-intercalated $Li_{4+x}Ti_5O_{12}$ nanocrystals can contain the (111) phase boundary.

The atomic structure of Zr-doped c-LTO is shown in Figure 7 (Appendix). Here, the Zr atom substitutes Ti in the c-LTO lattice.

The electronic properties and band structure of c-LTO–Zr along high symmetry points were calculated using the DFT SGGA+U method (U_{eff} = 4 eV, O 2*p*, Ti *3d*, Zr 4*d*) (Figure 8, Appendix).

Taking into account the spin states of DFT SGGA+U (U_{eff} = 4 eV, O 2*p*, Ti *3d*, Zr 4*d*), the energy of the forbidden band calculated by us in the band structure of lightly doped c-LTO–Zr (c-$Li_4Ti_{4.99}Zr_{0.01}O_{12}$) had the following value: $E_g\uparrow$= 2.68 eV and $E_g\downarrow$ = 1.95 eV. For the band structure of the lightly doped c-LTO–Zr supercell, the valence band maximum (VBM) is located at the Γ point, while heavy doping can shift the conduction band minimum (CBM) towards the X point.

Heavy doping of a c-LTO–Zr can lead to the fact that the transition of an electron between the conduction band and the valence band (Γ–X) can be accompanied by a change in momentum, i.e. an indirect transition can take place. With such an indirect transition, an indirect form of the forbidden zone is obtained in the quasi-momentum space between the valence band and the conduction band of the lattice of the substance. The transition of an electron between zones in a c-LTO–Zr structure can be accompanied by a change in its momentum, carried away by an additional particle, for example, a phonon.

Thus, the DFT SGGA+U calculated band gap energy of lightly doped c-LTO–Zr is on average 2.32 eV. This value is consistent with calculations [23] and lower than the experimental value of 3.55 eV, [24]. The calculated total DOS and partial densities of states PDOS for c-LTO–Zr are shown in Figure 9 (Appendix), a, b. DFT SGGA+ U calculated the partial magnetic moment of zirconium in $Li_4Ti_{4.99}Zr_{0.01}O_{12}$ is 1.002 μ_B.

3.6 Electronic Structure of c-LTO–Nb

The atomic structure of c-LTO–Nb is shown in Figure 10. Here, the Nb atom substitutes Ti in the c-LTO lattice.

The results of DFT SGGA+*U* calculations of the electronic properties of c-LTO–Nb along the high symmetry points are shown in Figure 11.

In the band structure of c-LTO–Nb, the valence band maximum (VBM) is located at the Γ point, as in c-LTO–Zr, and the conduction band minimum (CBM) is slightly shifted towards the X point due to light doping. The electron transition between the conduction and valence bands (Γ–X) under such doping is a direct transition.

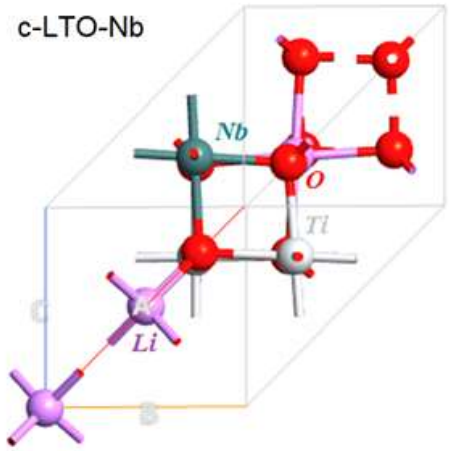

Fig. 10: Atomic structure of doped c-LTO–Nb. The Nb atom substitutes Ti in the lattice c-$Li_4Ti_{5-x}Nb_xO_{12}$

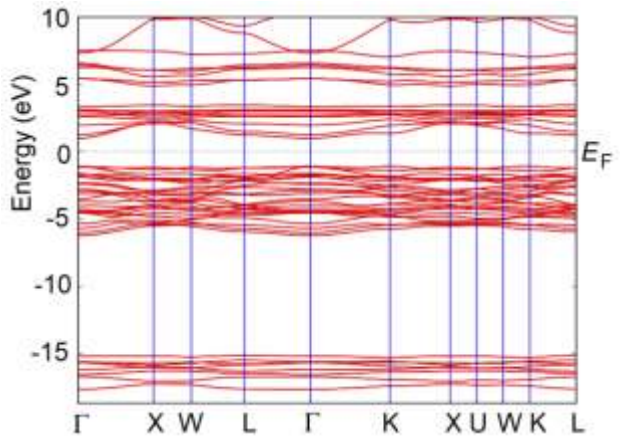

Fig. 11. Calculated DFT SGGA+*U* (U_{eff} = 4 eV, O 2*p*, Ti 3*d*, Nb 4*d*) band structure of c-LTO–Nb, where the Nb atom substitutes the Ti atom in the c-$Li_4Ti_{4.99}Nb_{0.01}O_{12}$ lattice

The calculated SGGA+*U* band gap energy of c-LTO–Nb was E_g = 2.09 eV. The total DOS and partial densities of states PDOS for c-LTO–Nb are shown in Appendix in Figure 12(a), and Figure 12(b).

The observed sharp peaks in the DOS spectra arise from the ground spin states of Ti 3*d* and the impurity Zr(Nb) 4*d*. The spin states of Ti and Zr(Nb) are strongly localized in c-LTO–Zr(Nb) because their energy width is small. The difference in energy between the spin states of *s*, *p*, and *d* electrons arises from the contribution of the Hubbard parameter (U_{eff} = 4 eV) to the calculations. The value of U_{eff} = 4 eV used for Ti 3*d* and Zr(Nb) 4*d* in the DFT SGGA+*U* calculations shifts the minority spin states of *d* electrons near the Fermi energy. This is probably why the non-ground spin states of *d*-electrons have low energy, and electrons can be excited in them.

Therefore, these minor spin states can be filled with electrons and affect the physical properties of c-LTO–Zr(Nb). DFT SGGA+*U* calculated the local partial magnetic moment of niobium is ~0 μ_B with Nb(Ti) substitution in c-$Li_4Ti_{4.99}Nb_{0.01}O_{12}$ lattice.

3.7 Conductivity of Doped c-LTO–Zr

$Li_4Ti_{5-x}Zr_xO_{12}$ (x = 0.05, 0.1, 0.2) electrodes have better electronic and ionic conductivity than the undoped LTO electrode. This is indicated by the results of the electrochemical study of $Li_4Ti_{5-x}Zr_xO_{12}$, [16]. For example, for the optimal $Li_4Ti_{5-x}Zr_xO_{12}$ sample with a composition of 0.1 Zr, the charge transfer resistance and the solution resistance are 2.0 and 99.6 Ohm, respectively.

The $Li_4Ti_{5-x}Zr_xO_{12}$ electrode containing a doping impurity of 0.1 Zr possesses better electronic conductivity and ionic conductivity. With heavy doping, part of the Zr impurity cannot substitute Ti in the c-LTO lattice. This prevents the transport of Li ions and electrons in c-LTO–Zr. Thus, the lithium-ion conductivity and electronic conductivity of c-LTO-Zr, compared to c-LTO (Figure 13) is reduced. Electrodes made of c-LTO–Zr compositions have similar redox characteristics. This indicates that light Zr doping has little effect on the parameters of the electrochemical reaction involving the c-LTO–Zr anode. Doped $Li_4Ti_{5-x}Zr_xO_{12}$ (x = 0, 0.05, 0.1, 0.2) samples also have high discharge capacity and cyclic stability at the rate of 0.5C and 1.0C compared to pure c-LTO. With an increase in the rate from 0.5C, 1C, 3C, 5C, and 10C to 20C, the capacity of c-LTO–Zr decreased rapidly, [16], [26].

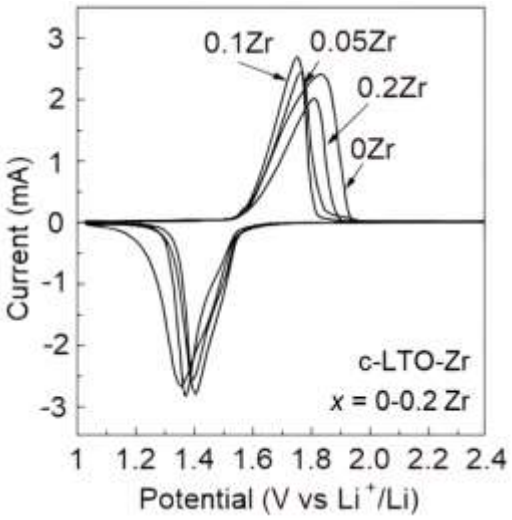

Fig. 13: Cyclic volt-ampere characteristics of $Li_4Ti_{5-x}Zr_xO_{12}$ samples (x = 0, 0.05, 0.1, 0.2). Scan rate: 0.2 mV/s, [16]

3.8 Conductivity of c-LTO–Nb

The c-LTO–Nb electrode has a higher specific capacity and better cycling performance than the LTO electrode. The c-LTO–Nb electrode exhibits a high charge rate with a reversible capacity of 135 mAh/g at 1C, 127 mAh/g at 20C, and 80 mAh/g at 40C.

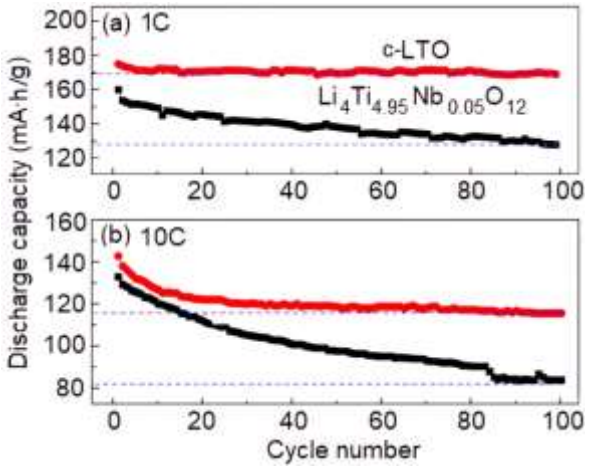

Fig. 14: Cycling characteristics of c-LTO and $Li_4Ti_{4.95}Nb_{0.05}O_{12}$ at (a) 1C and (b) 10C, [27]

The conductivity of doped samples is also improved (Figure 14). The conductivity of $Li_4Ti_{4.95}Nb_{0.05}O_{12}$ and c-LTO is 1.127×10^{-9} and 6.615×10^{-10} S/cm, respectively, [27]. The conductivity of $Li_4Ti_{4.95}Nb_{0.05}O_{12}$ also has a higher electrical conductivity than that of LTO, [28]. At room temperature, the conductivity of $Li_4Ti_{4.95}Nb_{0.05}O_{12}$ is higher (2×10^{-5} S/cm) than that of c-LTO (1.87×10^{-6} S/cm).

4 Conclusions

The compound of the composition $Li_4Ti_5O_{12}$ (c-LTO; cubic structure, space group – $Fd\bar{3}m$; spinel structure) is used as an anode (along with other high-voltage materials) in lithium-ion batteries (LIB). However, c-LTO crystals as an anode have disadvantages in their electronic, energy, and cyclic characteristics. Our calculations allow us to conclude that doping with *d*-elements improves the structural and electrical properties of c-LTO crystals.

This paper presents the results of DFT SGGA+U 2 × 2 × 2 supercell calculations of cubic spinel of partially substituted particles (atoms and/or ions) of titanium on zirconium (niobium) particles c-LTO–Zr(Nb). Calculations of lightly doped nanocrystals c-LTO; $Li_4Ti_{4.99}Zr_{0.01}O_{12}$ and $Li_4Ti_{4.99}Nb_{0.01}O_{12}$ (x = 0–0.01) showed the following. Using the SGGA+U

functional (the effective Hubbard parameter was U_{eff}= 4 eV) and the spin polarization effect, it is possible to adequately describe the structures with localized states of Ti 3*d* and Zr(Nb) 4*d* orbitals in c-LTO–Zr(Nb).

The geometry of the crystal structure with the optimized lattice parameter of c-LTO (8.352 Å) and c-LTO–Zr(Nb) (8.362 Å) includes an interconnected network of Ti, Zr(Nb), and O layers in the form of $[TiO_6]$ and partially substituted octahedra $[Zr(Nb)O_6]$. The proximity of the particle sizes of titanium and 4*d* elements with partial substitution of titanium ions by zirconium (or niobium) particles in the c-LTO spinel structure does not significantly distort the c-LTO–Zr(Nb) structure.

The formation energy E_f = -3.11 eV for $Li_4Ti_{4.99}Zr_{0.01}O_{12}$ and $Li_4Ti_{4.99}Nb_{0.01}O_{12}$ calculated using DFT SGGA+U (U_{eff} = 4 eV, O 2*p*-, Ti 3*d*-, Zr 4*d*- and Nb 4*d*-orbital) differs little from the value E_f = –3.21 eV for the monoclinic modification of m-LTO calculated using the DFT LSDA method. The difference in E_f is associated both with the functional used and can be associated with a change in the distribution of Ti cations and Zr(Nb) impurity particles in the octahedral and tetrahedral voids of the c-LTO–Zr(Nb) unit cell.

The energy spectra of the position of the valence and conduction band edges relative to the vacuum level and the density of states DOS of electrons in c-LTO–Zr(Nb) indicate the following. DOS of c-LTO–Zr(Nb) crystals contains sharp peaks near the Fermi energy E_F. For the

compositions $Li_4Ti_{4.99}Zr_{0.01}O_{12}$ and $Li_4Ti_{4.99}Nb_{0.01}O_{12}$, this energy in DOS is about –1.7 eV.

The energy near E_F also includes the spin-orbit interaction (SOC) related to the spatial asymmetry of the states. The SOC arises from the ground spin states of the Ti $3d^2$, Zr $4d^2$ and Nb $4d^4$ orbitals. The SOC energy includes the exchange energy and the energy of the direct Coulomb interaction. The SOC energy depends on the energy of different spin configurations of the *d*-elements and the degree of partial substitution of Zr(Nb) particles for titanium particles. The ground spin states of the Ti 3*d* and Zr(Nb) 4*d* orbitals are strongly localized in c-LTO–Zr(Nb) because their energy width is small. At weak SOC, the transitions between singlet and triplet states of the polarized levels in c-LTO–Zr(Nb) can be preserved. The minority spin states of Zr(Nb) are limited by the energy range and are negligible in DOS. Increasing the degree of partial substitution of titanium atoms by 4*d* Zr(Nb) atoms can lead to the formation of an indirect forbidden transition in c-LTO–Zr(Nb).

DFT SGGA+U (U_{eff} = 4 eV, O 2*p*-, Ti 3*d*-, Zr 4*d*- and Nb 4*d*-orbital) calculated band gap E_g of doped c-LTO–Zr(Nb) structures with partial substitution of titanium by zirconium (or niobium) [Zr(Nb) →Ti] in the spin-up (↑) and spin-down (↓) states differ from each other. Calculations of c-LTO–Zr(Nb) give the following average values of E_g, eV: c-LTO 2.98 (x = 0), $Li_4Ti_{4.99}Zr_{0.01}O_{12}$ 2.32, $Li_4Ti_{4.99}Nb_{0.01}O_{12}$ 2.09.

The difference in the calculated energy between the two spin states (spin up ↑ and spin down ↓) is due to the parameter U_{eff} used for Ti 3*d*, Zr 4*d* and Nb 4*d* orbitals. Using U_{eff}= 4 eV affects the shift of the minority spin states near the Fermi energy. Since the minority spin states, for example in Ti 3*d* orbitals in c-LTO have relatively high energy, electrons cannot be potentially excited in them. However, the 4*d* orbitals of the dopant Zr(Nb) can fill the empty states of the Ti 3*d* orbitals, which will affect the physical properties of c-LTO–Zr(Nb).

Magnetic properties of a substance are usually determined by the magnetic properties of electrons and atoms (orbital motion of electrons; magnetic moment of an electron; magnetic moment of an atomic nucleus). The magnetic field caused by the magnetic moment of a nucleus is much smaller than the magnetic field created by the orbital motion of electrons and the spin of electrons.

Local magnetism in c-LTO–Zr(Nb) is formed by the contribution of spin energy (exchange energy and direct Coulomb interaction energy) to the total moment of an electron. When calculating the magnetic moment in c-LTO–Zr(Nb), the contribution of the spin magnetic moments of electrons forming the electron shell of Zr(Nb) atoms was taken into account. Thus, the local magnetic moment is the result of the spatial distribution of electrons and atoms of the c-LTO–Zr(Nb) cell, including impurity *d*-orbitals of Zr(Nb). The local magnetic moment of the partial 4*d*-orbitals of Zr(Nb) in the $Li_4Ti_{4.99}Zr_{0.01}O_{12}$ and $Li_4Ti_{4.99}Nb_{0.01}O_{12}$ compounds calculated by the DFT SGGA + U (U_{eff} = 4 eV) had the following values: 1.002 μ_B with [Zr→Ti] substitution and ~0 μ_B with [Nb→Ti] substitution. An increase in the degree of substitution of titanium particles by impurity Zr(Nb) particles affects the calculated magnetic moment of the partial components in c-LTO–Zr(Nb).

The known experimental results show that the alloyed c-LTO–Zr(Nb) materials possess improved electronic conductivity and electrochemical performance in LIB. c-LTO–Zr(Nb) anodes have higher specific capacity and better cyclic performance in LIB. For $Li_4Ti_{4.95}Nb_{0.05}O_{12}$, the capacity is 169.1 mAh/g at 1C and 115.7 mAh/g at 10C after 100 cycles, which is significantly higher than the capacity of the c-LTO anode. The maximum electronic conductivity corresponds to the $Li_4Ti_{4.95}Zr_{0.05}O_{12}$ and $Li_4Ti_{4.95}Nb_{0.05}O_{12}$ compositions. These compositions also have a higher lithium-ion diffusion coefficient compared to pure c-LTO.

One of the possible options for using the obtained DFT results of calculation of the structural properties of doped materials c-LTO–Zr(Nb) may be their application in difficult-to-obtain structures and areas where it is not possible to repeatedly synthesize a nanostructure with a given composition, to interfere with the formation of the desired polytype of the structure and physical properties of materials.

DFT results can be used to predict whether a given c-LTO–Zr(Nb) cubic structure will transform to another modification or polytype during LIB operation. Phase transitions in c-LTO–Zr(Nb) compounds can be associated with instability of the crystal lattice in the highly symmetric cubic phase. In this class of compounds, both homogeneous non-polar distortions of the crystal lattice and distortions associated with a change in the volume

of the unit cell of the crystal are observed in low-temperature phases. Using theoretical and DFT data, important physical properties of c-LTO–Zr(Nb) such as the density of electron states, bulk modulus, lattice constants, permittivity, electrical conductivity, and others can be further determined.

The practical value of the results is that, given a method for determining the morphology and structural parameters of batteries, the DFT calculation data can be used to warn the user before the physical parameters, including the crystal lattice parameters of the LTO electrode, are violated.

Such a forecast can save time and money for the manufacturer and the consumer to prevent failures in the operation of the electrochemical system containing c-LTO. Data on the patterns of change in physical and chemical properties during doping will enable the preparation for electrode damage, poor reproducibility, and failure situations in advance and ensure the smooth operation of c-LIB.

The obtained data can be used to evaluate the influence of other alloying elements on the structure, properties, design, and performance improvement problems of LIB. Using the modeling method with the fitting of physical and structural properties in the prediction process, it is possible to optimize the prediction performance and the operation of LIB.

References:

[1] H. Zhang, Y. Yang, H. Xu, L. Wang, X. Lu, and X. He," $Li_4Ti_5O_{12}$ Spinel Anode: Fundamentals and Advances in Rechargeable Batteries," *InfoMat*, vol. 4, no. 12228, pp. 1-19, 2022, https://doi.org/10.1002/inf2.12228.

[2] C.-H. Chen, J.-M. Chiu, I. Shown, and C.-H. Wang, "Development of a Lightweight LTO/Cu Electrode as a Flexible Anode via Etching Process for Lithium-Ion Batteries," *American Chemical Society, (ACS) Omega*, vol. 7, pp. 10205-10211, 2022, https://doi.org/10.1021/acsomega.1c06704.

[3] P.V. Kornev, T.L. Kulova, A.A. Kuzmina, E.K. Tusseeva, A.M. Skundin, V.M. Klimova, and E.S. Koshel, "Europium-Doped Lithium Titanate as a Material for the Anodes of Lithium-Ion Batterie," *Russian Journal of Physical Chemistry* A, vol. 96, pp. 435-441, Mar. 2022, https://doi.org/10.1134/S0036024422020145.

[4] T.-F. Yi, L.-J. Jiang, J. Shu, Cai-Bo Yue, Rong-Sun Zhu, and Hong-Bin Qiao, "Recent Development and Application of $Li_4Ti_5O_{12}$ as Anode Material of Lithium Ion Battery," *Journal of Physics and Chemistry of Solids*, vol. 71, no. 9, pp. 1236-1242, May. 2010, https://doi.org/10.1016/j.jpcs.2010.05.001.

[5] V.I. Ivanenko, M.V. Maslova, G.B. Kunshina, S.V. Vladimirova, and D.V. Agafonov, 'Lanthanum(III)-Doped $Li_4Ti_5O_{12}$-Based Nanostructured Anode Material for Lithium-Ion Current Sources," *Protection of Metals and Physical Chemistry of Surfaces*, vol. 56, pp. 951-956, 2020, https://doi.org/10.1134/S2070205120040139.

[6] J. Gao, I. Ying, C. Jiang, and C. Wan, "Preparation and Characterization of Spherical La-Doped $Li_4Ti_5O_{12}$ Anode Material for Lithium Ion Batteries," *Ionics*, vol. 15, pp. 597-601, Dec. 2009, https://doi.org/10.1007/s11581-008-0306-0.

[7] D. Wang, C. Zhang, Y. Zhang, J. Wang, and D. He, "Synthesis and Electrochemical Properties of La-Doped $Li_4Ti_5O_{12}$ as Anode Material for Li-Ion battery," *Ceramics International*, vol. 39, pp. 5145-5149, Dec. 2013, https://doi.org/10.1016/j.ceramint.2012.12.010.

[8] L. Yao, Z. Ning, S. Guo, Y. Guo, Y. Sun, C.R. Rambo, T. Yuan, Z. Huang, C. Zhang, and D. He, "On the Sol-gel Synthesis Mechanism of Nanostructured $Li_{3.95}La_{0.05}Ti_{4.95}Ag_{0.05}O_{12}$ with Enhanced Electrochemical Performance for Lithium Ion Battery," *Ceramics International*, vol. 43, no. 3, pp. 3393–3400, Nov. 2017, https://doi.org/10.1016/j.ceramint.2016.11.185.

[9] J. Gao, C. Jiang, and C. Wan, "Synthesis and Characterization of Spherical La-Doped Nanocrystalline $Li_4Ti_5O_{12}$/C Compound for Lithium-Ion Batteries," *Journal of the Electrochemical Society*, vol. 157, no. 2, pp. K39-K42, Dec. 2010, https://doi.org/10.1149/1.3265458.

[10] M. Knapp, H. Ehrenberg, G. Chen, Z. Shen, G. Yang, L. Gu, and F. Du, "Lithium Lanthanum Titanate Perovskite as an Anode for Lithium Ion Batteries," *Natural Communications*, vol. 11, no. 3490, 2020, https://doi.org/10.1038/s41467-020-17233-1.

[11] Z. Wang, W. Yang, J. Yang, L. Zheng, K. Sun, D. Chen, L. Sun, X. Liu, "Tuning the Crystal and Electronic Structure of $Li_4Ti_5O_{12}$ via Mg/La Cooping for Fast and Stable Lithium Storage," Ceramics International, vol. 46, no. 9, pp. 12965-12974, Jun. 2020, https://doi.org/10.1016/j.ceramint.2020.02.066.

[12] Z. Zhang, R. Xun, L. Wang,and Z. Meng, Construction of Pseudocapacitive $Li_{2-x}La_xZnTi_3O_8$ Anode for Fast and Super-Stable Lithium Storage," *Ceramics International*, vol. 47, no. 1, pp. 662-669, Jan. 2021, https://doi.org/10.1016/j.ceramint.2020.08.174.

[13] G. Wei, C.R. Rambo, Y. Guo, Z. Ning, S. Guo, M. Zhao, Z. Huang, C. Zhang, and D. He, "Graphene Coated La^{3+}/Sc^{3+} co-Doped $Li_4Ti_5O_{12}$ Anodes for Enhanced Li-ion Battery Performance," *Materials Letters*, vol. 193, pp. 179-18, Apr. 2017, https://doi.org/10.1016/j.matlet.2017.01.082.

[14] M.R. Sovizi and S.M. Pourali, "Effect of Praseodymium Doping on Structural and Electrochemical Performance of Lithium Titanate Oxide ($Li_4Ti_5O_{12}$) as New Anode Material for Lithium Sulfur Batteries," *Journal of Electronic Materials*, vol. 47, pp. 6525-653, Aug. 2018, https://doi.org/10.1007/s11664-018-6552-7.

[15] Q. Zhang and X. Li, "High Rate Capability of Nd-Doped $Li_4Ti_5O_{12}$ as an Effective Anode Material for Lithium-Ion Battery," *International Journal of Electrochemical Science*, vol. 8, no. 6, pp. 7816-7824, Jun. 2013, https://doi.org/10.1016/S1452-3981(23)12848-3.

[16] X. Li, M. Qu, and Z. Yu, "Structural and Electrochemical Performances of $Li_4Ti_{5-x}Zr_xO_{12}$ as Anode Material for Lithium-Ion Batteries," *Journal of Alloys and Compounds*, vol. 487, no. 1-2, pp. L12-L17, Jul. 2009, https://doi.org/10.1016/j.jallcom.2009.07.176

[17] M.M. Asadov, S.O. Mammadova, S.N. Mustafaeva, S.S. Huseynova, and V.F. Lukichev, "Modeling of the Electronic Properties of M-Doped Supercells $Li_4Ti_5O_{12}$–M (M = Zr, Nb) with a Monoclinic Structure for Lithium-Ion Batteries," *Russian Microelectronics*, vol. 53, no. 1, pp. 1-13, Jan. 2024, https://doi.org/10.1134/S1063739723600127.

[18] L. Hou, X. Qin, X. Gao, T. Guo, H. Li, and J. Li, "Zr-Doped $Li_4Ti_5O_{12}$ Anode Materials with High Specific Capacity for Lithium-Ion Batteries," *Journal of Alloys and Compounds*, vol. 774, pp. 38-45, Feb. 2019, https://doi.org/10.1016/j.jallcom.2018.09.364

[19] B. Tian, H. Xiang, L. Zhang, Z. Li, and H. Wang. "Niobium Doped Lithium Titanate as a High Rate Anode Material for Li-Ion Batteries," *Electrochimica Acta*, vol. 55, no. 19, pp. 5453-5458, Apr.2010, https://doi.org/10.1016/j.electacta.2010.04.068.

[20] B. Vikram Babu, M. Sushma Reddi, K. Surendra, A. Rama Krishna, K. Samatha, and V. Veeraiah, "Synthesis, Characterization and Electrical Studies of Nb-Substituted $Li_4Ti_5O_{12}$ Anode Materials for Li-Ion Batteries," *Materials Today: Proceedings*, vol. 43, no. 2, pp. 1485-1490, Sep. 2021, https://doi.org/10.1016/j.matpr.2020.09.310.

[21] J.P. Perdew, K. Burke, and M. Ernzerhof, "Generalized Gradient Approximation Made Simple," Physical Review Letters, vol. 77, pp. 3865-3868, Oct. 1996, https://doi.org/10.1103/physrevlett.77.3865.

[22] J.P. Perdew, A. Ruzsinszky, G.I. Csonka, O.A. Vydrov, G.E. Scuseria, L.A. Constantin, X. Zhou, and K. Burke, "Restoring the Density-Gradient Expansion for Exchange in Solids and Surfaces," Physical Review Letters, vol. 100, pp. 13640-6, Apr. 2008, https://doi.org/10.1103/PhysRevLett.100.136406.

[23] V.I. Anisimov, F. Aryasetiawan and A.I. Lichtenstein, "First-Principles Calculations of the Electronic Structure and Spectra of Strongly Correlated Systems: the LDA+U Method," Journal of Physics: Condensed Matter, vol. 9, pp. 767-808, Jan. 1997, https://doi.org/10.1088/0953-8984/9/4/002.

[24] S.M. Asadov, S.N. Mustafaeva, S.S. Huseinova, and V.F. Lukichev, "Simulation of Electronic Properties, Enthalpy of Formation, and Dielectric Characteristics of Yb-Doped Single Crystal $TlInS_2$," *Russian Journal of Physical Chemistry* A, vol. 98, no. 1, pp. 1-8, Jan. 2024, https://doi.org/10.1134/S0036024424010023.

[25] A. Khaparde, V. Deshmukh, V. Sharma, and U. Singh, "Li-Ion Battery Temperature Forecasting Method:Case-Study," *WSEAS Transactions on Electronics*, vol. 14, pp. 112-121, 2023, https://doi.org/10.37394/232017.2023.14.13

[26] C.Y. Ouyang, Z.Y. Zhong, and M.S. Lei, "Ab initio Studies of Structural and Electronic Properties of $Li_4Ti_5O_{12}$ Spinel," *Electrochemistry Communications*, vol. 9, no. 5, pp. 1107-1112, May 2007, https://doi.org/10.1016/j.elecom.2007.01.013

[27] L. Sarantuya, N. Tsogbadrakh, E. Enkhjargal, P. Altantsog, G. Sevjidsuren, and A. Pagvaja, "Structural and Electronic Properties of the Spinel $Li_4Ti_5O_{12}$," *Mongolian Journal of Chemistry*, vol. 20, no. 46, pp. 7-12, 2019, https://doi.org/10.5564/mjc.v20i46.1236.

[28] Y. Tanaka, M. Ikeda, M. Sumita, T. Ohno, and K. Takada, "First-Principles Analysis on Role of Spinel (111) Phase Boundaries in $Li_{4+3x}Ti_5O_{12}$ Li-ion Battery Anodes," *Physical Chemistry Chemical Physics*, vol. 18, pp. 23383-23388, Aug. 2016, https://doi.org/10.1039/c6cp04131k

Contribution of Individual Authors to the Creation of a Scientific Article (Ghostwriting Policy)

- Mirsalim Asadov, Solmaz Mustafaeva, Saida Mammadova equally contributed in the present research, at all stages from the formulation of the problem to the final findings and solution.
- Esmira Kuli-Zade and Vladimr Lukichev was responsible for the Statistics.

Sources of Funding for Research Presented in a Scientific Article or Scientific Article Itself

No funding was received for conducting this study.

Conflict of Interest

The authors have no conflicts of interest to declare.

APPENDIX

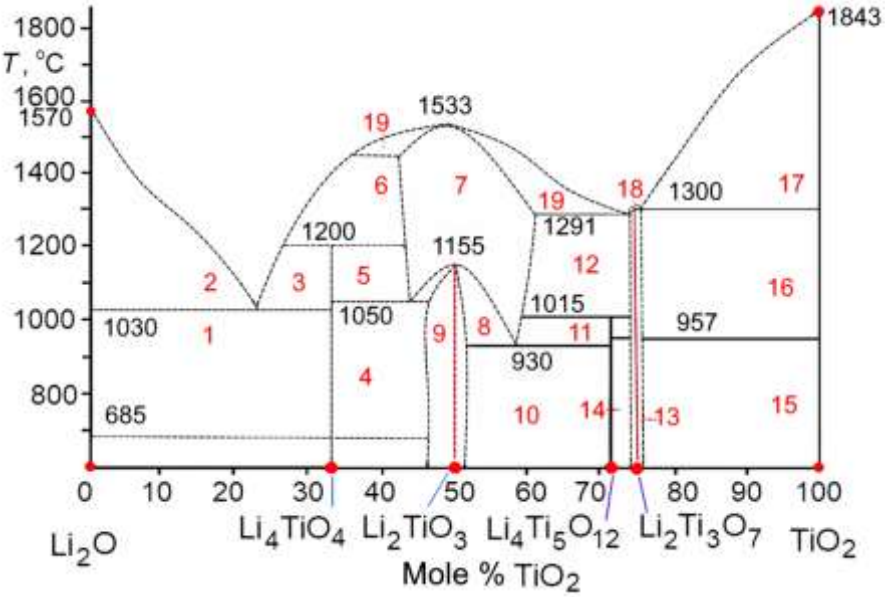

Fig. 1: Refined phase diagram of the system $Li_2O - TiO_2$. 1 – $Li_2O +$ Li_4TiO_4; 2 – $Li_2O +$ L (liquid); 3 – L + Li_4TiO_4; 4 – $Li_4TiO_4 +$ $\beta - Li_2TiO_3$ (ss), where ss – solid solutions; 5 – $Li_4TiO_4 +$ $\gamma - Li_2TiO_3$ (ss); 6 – L + $\gamma - Li_2TiO_3$ (ss); 7 – $\gamma - Li_2TiO_3$ (ss); 8 – $\gamma - Li_2TiO_3$ (ss) + $\beta - Li_2TiO_3$; 9 – $\beta - Li_2TiO_3$ (ss); 10 – $\beta - Li_2TiO_3$ (ss) + m – $Li_4Ti_5O_{12}$ (m – LTO); 11 – $\gamma - Li_2TiO_3$ (ss) + c – LTO ; 12 – $\gamma - Li_2TiO_3$ (ss) + $Li_2Ti_3O_7$; 13 – $Li_2Ti_3O_7$ (ss); 14 – $\beta - Li_2Ti_3O_7$ (ss) + m – LTO; 15 – $\beta - Li_2Ti_3O_7$ (ss) + TiO_2; 16 – $\gamma - Li_2Ti_3O_7$ (ss) + TiO_2; 17 – L + TiO_2; 18 – $\gamma - Li_2Ti_3O_7$ (ss) + L; 19 – $\gamma - Li_2TiO_3$ (ss) + L

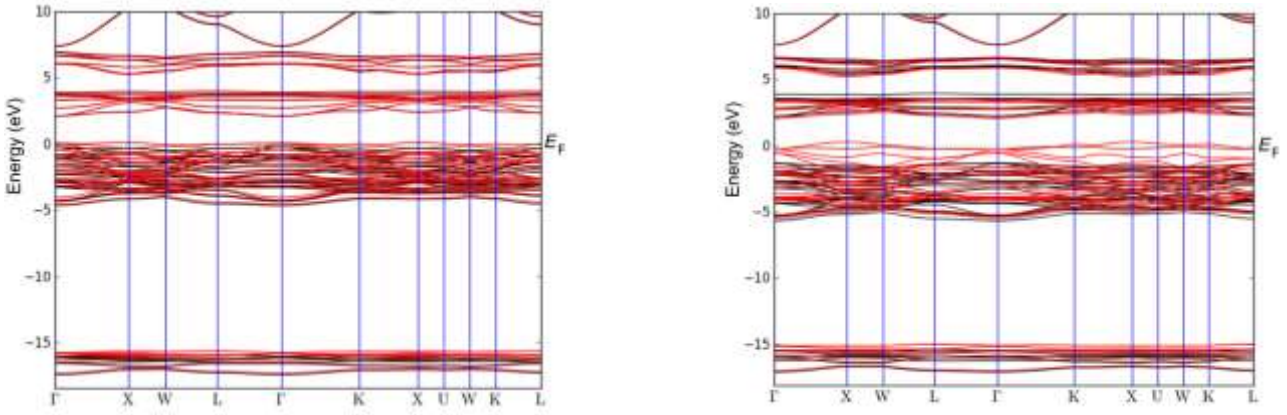

~~a)~~ (a) ~~b)~~(b)

Fig. 4: Calculated band structure in a 2 × 2 × 2 supercell of c-LTO spinel. ~~a)~~(a) DFT LSDA calculation, ~~b)~~(b) DFT SGGA+U calculation (U_{eff} = 4 eV, for 2p electrons of O, 3d electrons of Ti). In the calculations, only local exchange integrals for 2p- and 3d-electrons (*p-d and d-d* model) were taken into account. Zero of the energy scales corresponds to E_F, i.e., the Fermi level is 0

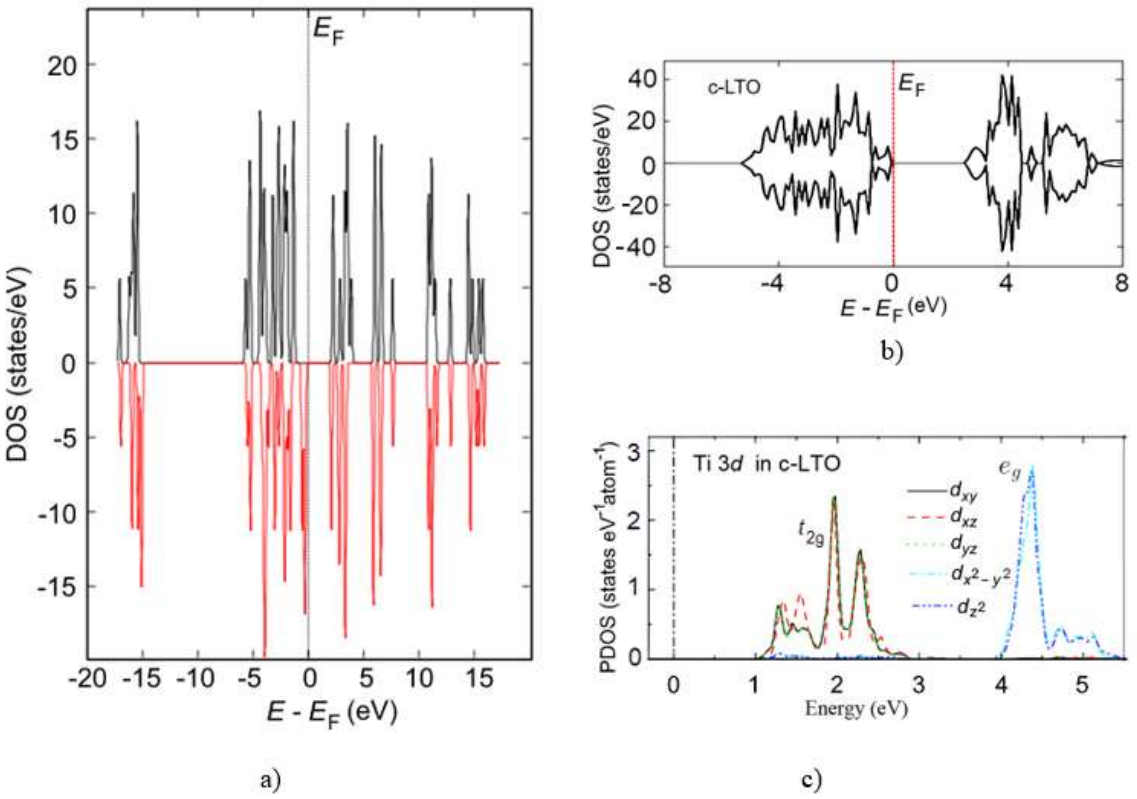

Fig. 5: Density of states of atoms in the 2 × 2 × 2 spinel supercell of c-LTO. ~~a~~)(a) DOS of the c-LTO cell calculated by the DFT SGGA+U method (U_{eff} = 4 eV, O 2p, Ti 3d). (b) DOS of c-LTO, [28]. (c) PDOS of Ti in c-LTO [26]. Zero of the energy scales corresponds to E_F, i.e., the Fermi level is 0

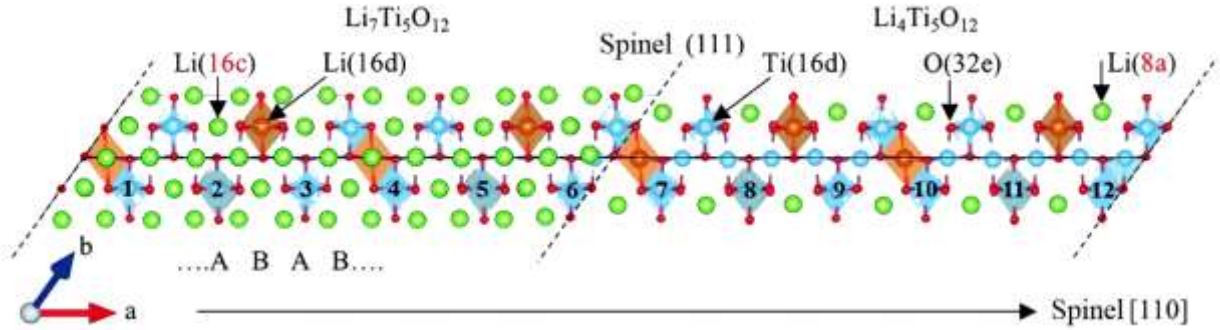

Fig. 6: Structure of the two-phase model c-LTO/$Li_7Ti_5O_{12}$ with (111) interface planes as phase boundaries (dashed lines), [28]. In the Ti–O framework, the Li filling sites vary from 8a in c-LTO to 16c in $Li_7Ti_5O_{12}$. The TiO_6 octahedra have a stacking sequence ABAB. . . along the <111> spinel directions in the cell

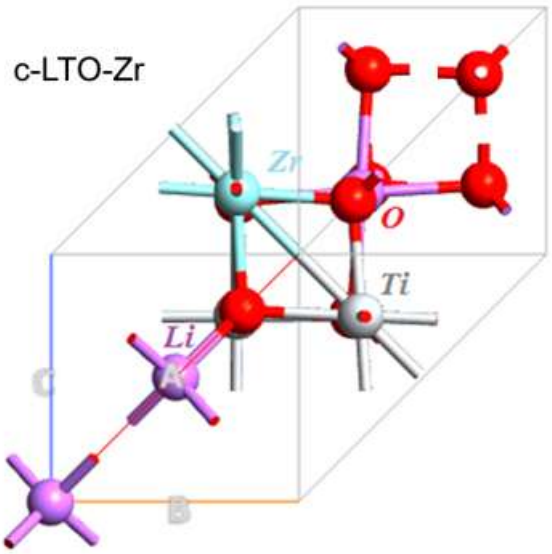

Fig. 7: Atomic structure of Zr-doped c-LTO–Zr. The Zr atom substitutes Ti in the lattice c-$Li_4Ti_{5-x}Zr_xO_{12}$

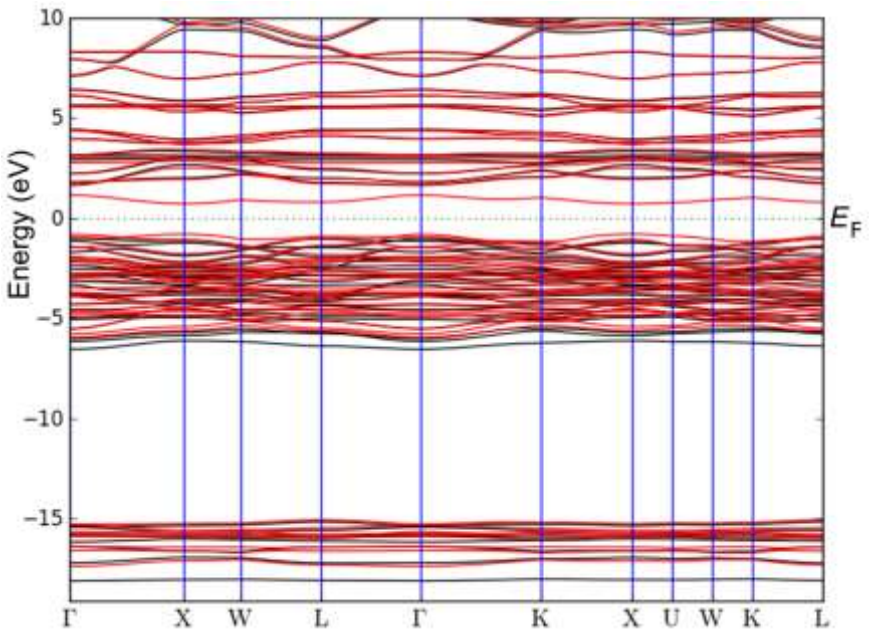

Fig. 8: DFT SGGA+U (U_{eff} = 4 eV, O 2p, Ti 3d, Zr 4d) calculated band structure of the 2 × 2 × 2 supercell of c-LTO–Zr spinel, where the Zr atom substitutes the Ti atom in the lattice c- $Li_4Ti_{4.99}Zr_{0.01}O_{12}$. Zero of the energy scales corresponds to E_F, i.e., the Fermi level is 0

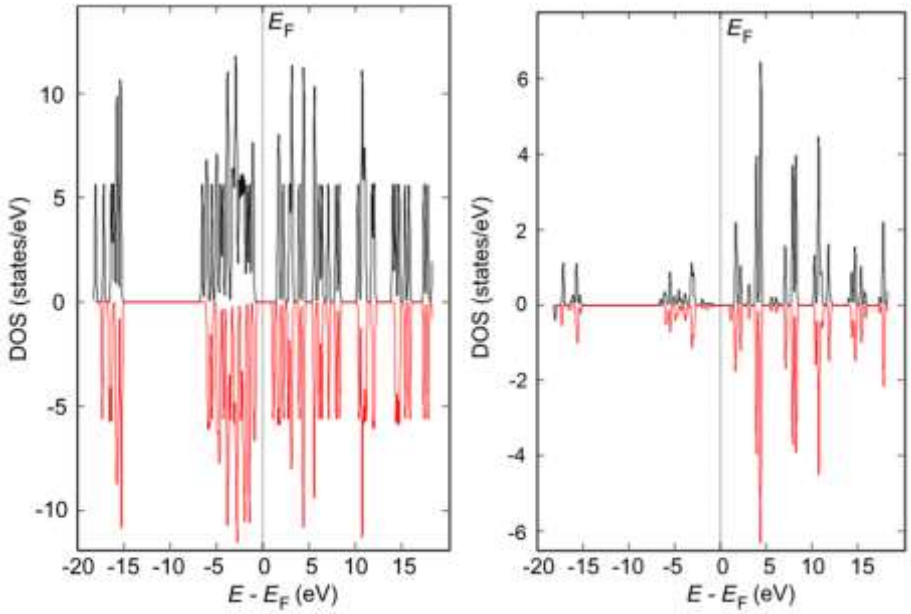

Fig. 9: Spin-allowed, total DOS (a) and partial density of states (PDOS) of *d*-states in c-$Li_4Ti_{4.99}Zr_{0.01}O_{12}$ (b)

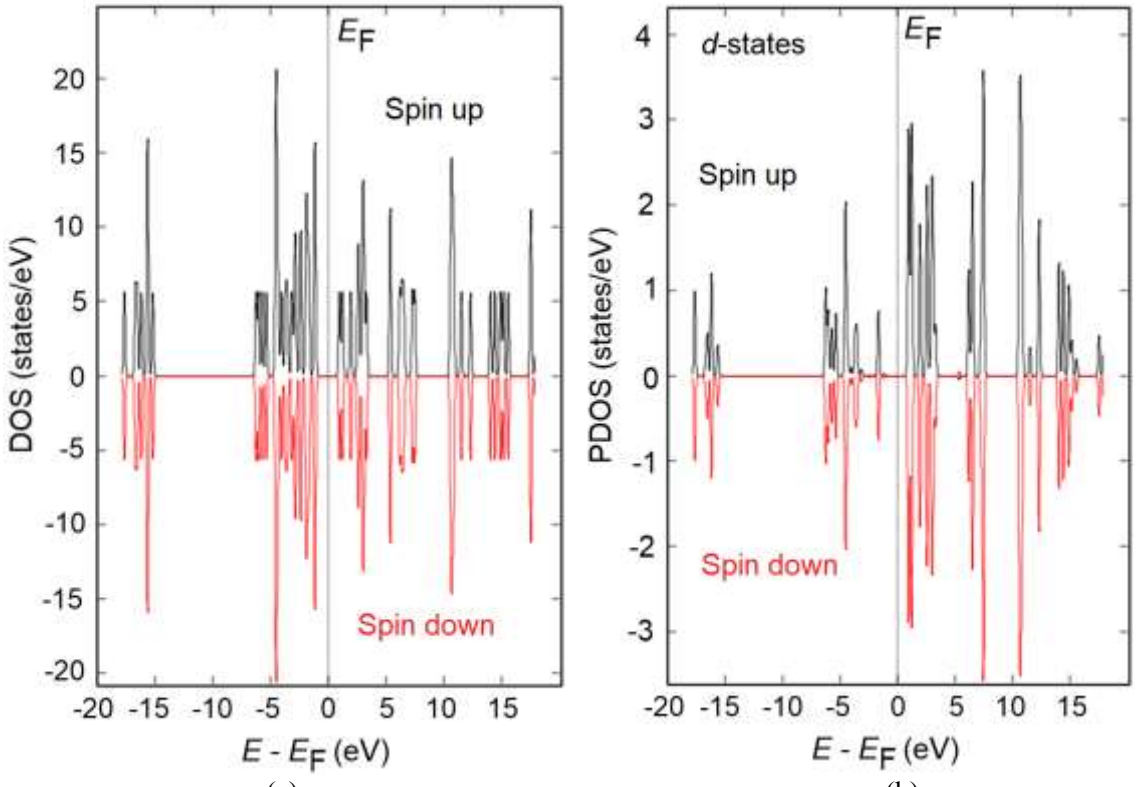

Fig. 12: Calculated by DFT SGGA+*U* (U_{eff} = 4 eV, O 2*p*, Ti 3*d*, Nb 4*d*) total density of states (a) and atomic-partial density of *d*-states (PDOS) in c-$Li_4Ti_{4.99}Nb_{0.01}O_{12}$ (b) for the energy range from −16 to 16 eV